On the deformation mechanisms and electrical behavior of highly stretchable metallic interconnects on elastomer substrates

Yeasir Arafat, Indranath Dutta, and Rahul Panat[a)]
School of Mechanical and Materials Engineering, Washington State University, Pullman, Washington 99163, USA

(Received 12 July 2016; accepted 28 August 2016; published online 16 September 2016)

Flexible metallic interconnects are highly important in the emerging field of deformable/wearable electronics. In our previous work [Arafat *et al*., Appl. Phys. Lett. **107**, 081906 (2015)], interconnect films of Indium metal, periodically bonded to an elastomer substrate using a thin discontinuous/cracked adhesion interlayer of Cr, were shown to sustain a linear strain of 80%–100% without failure during repeated cycling. In this paper, we investigate the mechanisms that allow such films to be stretched to a large strain without rupture along with strategies to prevent a deterioration in their electrical performance under high linear strain. Scanning Electron Microscopy and Digital Image Correlation are used to map the strain field of the Cr adhesion interlayer and the In interconnect film when the elastomer substrate is stretched. It is shown that the Cr interlayer morphology, consisting of islands separated by bi-axial cracks, accommodates the strain primarily by widening of the cracks between the islands along the tensile direction. This behavior is shown to cause the strain in the In interconnect film to be discontinuous and concentrated in bands perpendicular to the loading direction. This localization of strain at numerous periodically spaced locations preempts strain-localization at one location and makes the In film highly stretchable by delaying rupture. Finally, the elastic-plastic mismatch-driven wrinkling of the In interconnect upon release from first loading cycle is utilized to delay the onset of plasticity and allow the interconnect to be stretched repeatedly up to 25% linear strain in subsequent cycles without a deterioration of its electrical performance. *Published by AIP Publishing*. [http://dx.doi.org/10.1063/1.4962453]

I. INTRODUCTION

Flexible electronic devices are used in several emerging applications such as robotic skins,[1] electronic eye,[2] epidermal electronics,[3] smart clothing,[4] medical diagnostics,[5] sportswear,[6] and bendable displays.[7–9] The proliferation of such devices is predicted to lead to the "Internet of Things" (IoT) revolution over the next two decades.[3] A flexible electronic device typically consists of small islands of hard materials such as logic chips, chipsets, sensors, and other peripherals, connected by flexible conductors.[10–13] These conductors are metallic films having a thickness of $>1\,\mu$m and a width of about 10–50 μm and are expected to undergo numerous, large cyclic tensile and flexural strain without failure or reduction of electrical performance. Existing methods to improve interconnect stretch-ability without substantially degrading the electrical properties include creating serpentine structures of metal films,[14–21] non-planar buckling structures,[10,11,22,23] or other in-plane geometries.[24] However, serpentine circuitry is space-inefficient and is more resistive because of the increased length, requiring larger/bulky batteries that are incompatible with flexible device applications. Additionally, imposing strains by straightening of serpentines cause delamination of Cu thin films from the substrate.[20,21,25,26] The non-planar buckling structures are also difficult to pattern for high density circuitry due to the challenges in lithography based techniques for such geometries.[27] It has been proposed that strong interfacial adhesion enhances ductility of the film.[28] Indeed, thin films on elastomers may be stretched beyond their bulk counterparts due to suppression of necking instability,[28–31] but it is also observed that non-serpentine Cu films on polyimide show severe cracking at strains above ~20%, even when strongly bonded to the substrate.[29] Thin Au films on elastomers have been stretched in excess of 20% when the metal-substrate interface is intact,[13,32–34] but for many applications Au is prohibitively expensive. A porous elastomer substrate is also shown to enhance the stretch-ability of metal films,[35] although such substrates are not compatible with current industry practice. These limitations have necessitated the development of alternative approaches, including new materials, interfaces, and manufacturing processes to enable the production of highly conductive, stretchable, and reliable metallic interconnects.

To address these challenges, the authors have recently developed an interfacial engineering approach to incorporate some of the solution strategies above and created highly stretchable Indium interconnect films (thickness of ~6 μm) on polydimethylsiloxane (PDMS) substrates, without geometric manipulations (e.g., creating helical or serpentine geometry).[36] The In interconnect film in this study sustained a linear strain of 80%–100% without failure during repeated cycling.[36] Note that our study included a 3–5 nm thick Cr adhesion interlayer, which had a cracked, discontinuous morphology. During stretching, the In film resistivity was observed to increase up to about 30% linear strain, followed by a plateau up to 100% linear strain.[36] This suggested that

[a)]Author to whom correspondence should be addressed. Electronic mail: Rahul.panat@wsu.edu

Reuse of AIP Publishing content is subject to the terms at: https://publishing.aip.org/authors/rights-and-permissions. Download to IP: 69.166.45.107 On: Fri, 16 Sep 2016 15:59:33

either recovery or dynamic recrystallization limited the growth of dislocation density even as the film deformed plastically. A geometrical effect of out-of-plane wrinkling upon release from the first stretching cycle was also observed in this study and was attributed to the strain mismatch between the film and the elastomer.[36]

In spite of the significant progress in understanding of the highly stretchable metal-elastomer systems, several questions need further clarification as follows:

(a) The adhesion interlayer between interconnect and substrate used in different stretchable systems is often brittle (e.g., Cr, Ti) and creates "channel" cracks[37] in the system. The effect of the channel cracks on the film cracking as a function of film properties needs to be identified in order to engineer high stretch-ability. For example, it was recently shown that the Cr interlayer cracks cause cracking in Cu interconnect films.[38] However, the effect of such cracks on more ductile interconnects, where significant crack tip blunting can prevent a build-up of stresses, needs to be investigated.
(b) The brittle discontinuous interlayer in the stretchable systems is expected to modify the local strain distribution for the interconnect system. The relationship between the interlayer morphology, interface deformation, and the load transfer in the system is yet unclear.
(c) It is well known that the serpentine interconnects, although space inefficient, delay the onset of plasticity (hence an increase in resistivity) under strain. On the other hand, recovery mechanisms (e.g., recrystallization) in low melting temperature films are expected to limit an increase in the resistivity.[36] Strategies to enable space efficient interconnect architectures that, when stretched, delay the onset of plasticity and initiate the recovery at lower strain remain to be identified.

The impetus to undertake the present work is two-fold. First, we aim to identify the mechanisms that allow a high linear stretchability in ductile films bonded to elastomer substrates that can answer the questions (a) and (b) above. We believe that identifying the role played by the adhesion interlayer is highly important because the existing models postulate that a strong interfacial adhesion throughout the plane is necessary to enhance the strain to failure,[28] while our earlier work had demonstrated that a periodically bonded film can stretch to a strain much higher than that for bulk.[36] Second, we desire an understanding of the strain mismatch between the heterogeneous components of stretchable systems and device engineering strategies that can prevent the electrical deterioration of such films under high strain. Success in addressing these questions is critical for the realization of stretchable interconnects with space efficient architectures under demanding industry requirements.[39]

In this paper, an experimental study is presented that investigates and elucidates the deformation mechanisms in metal/adhesion interlayer/elastomer systems. The results show that the adhesion interlayer morphology plays a central role in enabling the interconnect film stretchability. It is demonstrated that the discontinuous adhesion interlayer allows the relatively thick interconnect to expand freely in-between the interlayer islands as they separate along the crack lines to accommodate the global strain arising from the stretching of the elastomer. Finally, an engineering approach is presented that will allow such films to be used without a deterioration in their electrical properties up to at least 25% linear strain.

II. MATERIALS AND EXPERIMENTAL DETAILS

The elastomer substrate, interlayer, and interconnect materials selected in this study were PDMS, Cr, and In, respectively. PDMS elastomer was chosen because of its wide availability, high stretchability, low cost, and biocompatibility[40] and was prepared by mixing 10 parts of base to 1 part of agent (Sylgard 184 Silicone Elastomer Kit, Dow Corning, Auburn, MI), followed by continuous stirring for 3–5 min, degassing, and cure. Degassing was achieved by keeping the PDMS gel in a sonicator (Cole-Parmer Ultrasonic Bath, Cole Parmer, Inc., Vernon Hills, IL) for longer of 20 min or until no bubbles were observed. The cure was done in a box oven (Neytech Vulcan furnace, Model 3–550, Degussa-Ney Dental, Inc., Bloomfield, CT) for 3 h at 80 °C. The cured PDMS blocks were about 0.4 mm thick, and their surfaces were treated with atmospheric oxygen plasma (Atomflo™ 400, Surfx® Technologies LLC, Redondo Beach, CA) with a power of 100 W for 1 min. Note that plasma treatment of PDMS surfaces is known to activate the surface –SiOH groups that help create a strong bond with Cr.[41] A thin layer of Cr film (3–5 nm or 10 nm) followed by an In film (1 μm or 500 nm thick) was deposited on PDMS using DC magnetron sputtering (BOC Edwards Auto 306, Edwards Corp., Crowley, UK) at ambient chamber-temperature without actively heating or cooling the substrate. The sputtered In film served as a seed-layer and provided electrical continuity for subsequent electrodeposition of In on the discontinuous (i.e., cracked) Cr film. Indium film of about 5 μm was then electroplated using an Indium Sulfamate bath (Indium Corporation, Clinton, NY). The electrodeposited In film was rectangular with the dimensions of 16.5 mm × 6.4 mm. The PDMS samples were cut to have dog-bone shape to make them suitable for a tensile loading.

For strain mapping experiments, the samples were stretched using a mini tensile stage with an integrated micrometer that measured the movement of the grips. A Scanning Electron Microscope (SEM, FEI Quanta 200F, FEI, Inc, Hillsboro, OR) was used to take images of the Cr and In surfaces to map the strain. The deformation of the Cr was obtained by using a grid over the SEM images and physically measuring the deformation perpendicular to the loading direction. Images were taken and analyzed at five different locations, each at magnifications of 1000×, 2000×, 5000× to get sufficient statistical variation. The deformation map of the In film was obtained using SEM images at 2000× magnification along with Digital Image Correlation (DIC) analysis using Ncorr software (MATLAB based open-source DIC tool, Atlanta, GA).[42,43] The DIC software uses multiple images that are deformed within the same Field of View (FOV) with reference to the initially captured un-deformed image. To locate the same location after each step of tensile loading, a pre-existing pinhole in the In film was selected.

Reuse of AIP Publishing content is subject to the terms at: https://publishing.aip.org/authors/rights-and-permissions. Download to IP: 69.166.45.107 On: Fri, 16 Sep 2016 15:59:33

Three seeding points (common features in all the images) were manually selected as reference points to be traced for the images for corresponding pixel-to-pixel correlation at a pixel density of 4.3 pixel/μm. The DIC parameters selected for this experiment are given in Table I (also see Ncorr user manual[44]).

For stretching experiments that involved electrical performance of the In film, a custom cyclic testing device was used with 4-wire resistance measurement and $7^1/_2$ digit ohmmeter (Model 34420A, Keysight Technologies, Santa Rosa, CA). The strain rate was maintained at $\sim 1.3 \times 10^{-3}$/s. The strain values reported for In in the work correspond to the linear strain in the In film and were verified by the movement of the fiducial marks on the film surface during stretching.

Three sets of experiments were carried out in the current study. In the first set of experiments, a 10 nm thick Cr layer was deposited on PDMS substrate and its deformation was observed under SEM when the substrate was stretched. The thickness of Cr was chosen to be close to that used in our prior work[36] but provide clear SEM images of the deformed Cr when stretched. In the second set of experiments, strain was measured on the top surface of the In interconnect under the SEM and the deformation mapped using DIC. In this case, the sputter coated Cr interlayer was about 5 nm, the sputter coated seed In was about 0.5 μm, while the electroplated In was about 1.5 μm. In the third set of experiments, the resistivity change in the In interconnect was measured as a function of mechanical cycling for the samples having film thicknesses similar to that of our prior work,[36] i.e., a 5 nm Cr layer and 1 μm In layer were successively sputter deposited on PDMS, followed by a 5 μm electroplated layer of In.

III. RESULTS

A. Deformation of PDMS-Cr system

We first investigated the deformation of a simple system consisting of the adhesion interlayer deposited on the elastomer without the presence of the thick interconnect. This study could provide the strain field and load transfer at the interface of elastomer and adhesion interlayer. Note that the effect on the interconnect layer will be assessed in Section III B. The deposited Cr film morphology is shown in Fig. 1 and includes numerous random cracks that divided the thin film into islands at a length scale of about 5–15 μm. The cracks were approximately biaxial. In addition, the interlayer did not show any gaps or pinholes. Such film morphologies have been observed for metal films deposited on PDMS and attributed to the rise in the PDMS temperature during the initial part of the deposition process that results in a biaxial tension on metal film due to its coefficient of thermal expansion mismatch with PDMS.[34,36]

TABLE I. The *NCorr* software[44] parameters used for the DIC study in the current work.

Step analysis type[a]	Leap frog
Image correspondence	[0 1] [1 2] [2 3] [3 4] [4 5] [5 6] [6 7] [7 8]
RG-DIC radius[b]	18
Strain radius[c]	10
Subset spacing[d]	2
Correlation coefficient cut-off[e]	1.9934

[a]For high strain analysis, *Leap Frog* option was chosen to manually select the reference seeds for each image corresponding to the previous one.
[b]*RG-DIC Radius* was chosen to collectively choose a subset of pixels bound within a certain region for DIC analysis.
[c]*Strain Radius* was chosen after the DIC analysis to visualize the strain field, keeping the overall noise as minimum as possible.
[d]*Subset Spacing* was the distance between two neighbor points within a certain strain radius that regulates the resolution of the strain field.
[e]*Correlation Coefficient Cut-off* number was optimally chosen to eliminate inclusion of bad data points from the final strain field visualization.

The PDMS was then stretched in the mini-tensile stage, and the strain field on Cr surface was observed under SEM. In particular, we looked to answer the following questions: (i) What is the strain in Cr blocks/islands vs that in-between the islands? (ii) Does the strain fully recover after unloading? (iii) Does Cr film show an increase in crack density in response to the loading? and (iv) Does the Cr layer show signs of delamination?

Figures 1(a)–1(f) show representative SEM images of the Cr interlayer when the PDMS substrate is stretched to 0%, 7%, 14%, 21%, 28%, and 35% strain, respectively. The loading direction was as indicated in Fig. 1. All the images in Fig. 1 are captured at the same (2000×) magnification, with a common scale shown in Fig. 1(a). The PDMS-Cr interface is seen to deform by widening the distance between the Cr islands (dark regions in Fig. 1) as a function of the applied strain. Note that to avoid charging in the SEM, a 1–2 nm thick layer of Pd was deposited on the Cr islands prior to the application of load on the PDMS substrate. At PDMS strain of 28% and 35% (see Figs. 1(e) and 1(f)), wrinkles perpendicular to the loading direction can be observed due to the Poisson effect. Figures 2(a)–2(f) show the results at the same strain level as in Figs. 1(a)–1(f), respectively, but during the unloading part of the cycle. Upon full unload, the blocks of Cr are seen to fully recover their deformation with minimal gaps between the islands as in the as-deposited condition.

To compare the strain from the Cr island separation and the strain applied to PDMS substrate, a grid with 10 equally spaced parallel vertical lines was placed on each image using *ImageJ* software[45] (National Institute of Health, Bethesda, MD) and the separation between the islands (i.e., dark regions) along each line was then manually measured and its percentage of the vertical line determined. The strain derived from the separation of the islands as a function of the applied strain is shown in Fig. 3 for the loading and the unloading part of the cycles. It can be observed that for up to about 7% applied strain, the measured strain based on the gaps between the islands was only 2.5%. We attribute this mismatch to the adjustment of the soft PDMS film until it is fully under tension since the film loading was performed manually in the stretching device. At higher strain, however, the measured strain scaled approximately linearly with applied strain. Figure 3 also shows that the deformation is fully reversible upon unloading, confirming the observations in Fig. 2. The result in Fig. 3 establishes that the global (substrate) deformation is distributed throughout the PDMS

Reuse of AIP Publishing content is subject to the terms at: https://publishing.aip.org/authors/rights-and-permissions. Download to IP: 69.166.45.107 On: Fri, 16 Sep 2016 15:59:33

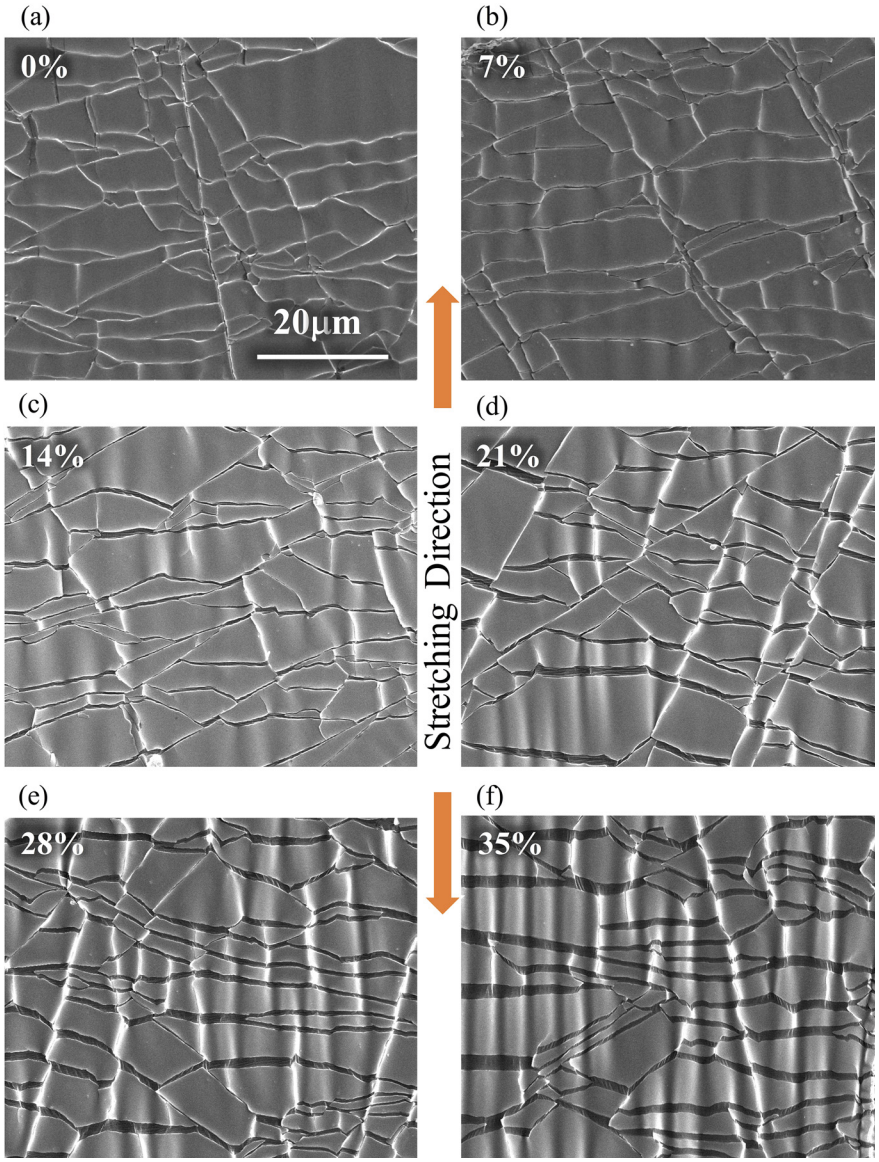

FIG. 1. Scanning Electron Microscope (SEM) images 10 nm thin Cr on PDMS with applied strain at different strain levels—(a) prior to stretching, (b) at 7% strain, (c) at 14% strain, (d) at 21% strain, (e) at 28% strain, and (f) at 35% strain. The widening of gaps between the Cr islands along the pulling direction is visualized through the darkened region on the surface. Wrinkles perpendicular to the loading direction are seen at strains of 28% and 35% due to the Poisson effect.

surface and that the movement of the Cr islands is responsible for the strain accommodation.

B. Deformation of PDMS-Cr-In system

Next, we obtained the strain field in the In interconnect for comparison with that for the Cr interlayer obtained in Section III A. The In interconnect thickness for this experiment was about 2 μm as described before. Figure 4 shows the representative SEM micrographs of the In surface along with overlaid surface strain maps for ε_{yy}, ε_{xx}, and ε_{xy}, obtained by the image analysis using the DIC software for applied strains of 0%, 7%, 21%, 35%, and 48%. The magnification of the images in Fig. 4 is the same as that for the Cr blocks shown in Figs. 1 and 2. The strain contours for each of the images in Fig. 4 are denoted by variable color codes. Since the sample substrate strain was uniaxial (along Y direction), the ε_{yy} plots shown in Fig. 4 are expected to be strongly influenced by the Cr interlayer. The ε_{yy} strain contours form discontinuous bands through the entire In film surface. The bands were perpendicular to the loading direction; and as expected, the magnitude of ε_{yy} increased as the applied strain increased. The spacing between successive bands indicating regions of high strain is about 5–15 μm. The ε_{xx} distribution in Fig. 4 is as expected and reflects the Poisson effect. Note that Figure 4 also shows the strain map of ε_{xy}, which is unremarkable. The results in Fig. 4 thus show that the In surface deforms in a discontinuous manner with high deformation bands perpendicular to the substrate loading direction. See also the visualizations of DIC results shown in Fig. 4 as online videos (Multimedia view).

To get an estimate/measure of the extent of localized strain (and hence deformation) in the In film shown in Fig. 4, ten parallel vertical lines were drawn per image using ImageJ software[45,46] to calculate the total width of the horizontal bands of high ε_{yy} strain. The "high" strain for this calculation was arbitrarily defined as a region with >60% of the maximum strain for a given image. Any other choice of "high" strain leads to a similar conclusion. Figure 5 shows the total width of the ε_{yy} bands of high strain on In surface and the total length of the gap between the Cr blocks (from Fig. 1) at applied strains of 0%, 7%, 21%, and 35%. From

Reuse of AIP Publishing content is subject to the terms at: https://publishing.aip.org/authors/rights-and-permissions. Download to IP: 69.166.45.107 On: Fri, 16 Sep 2016 15:59:33

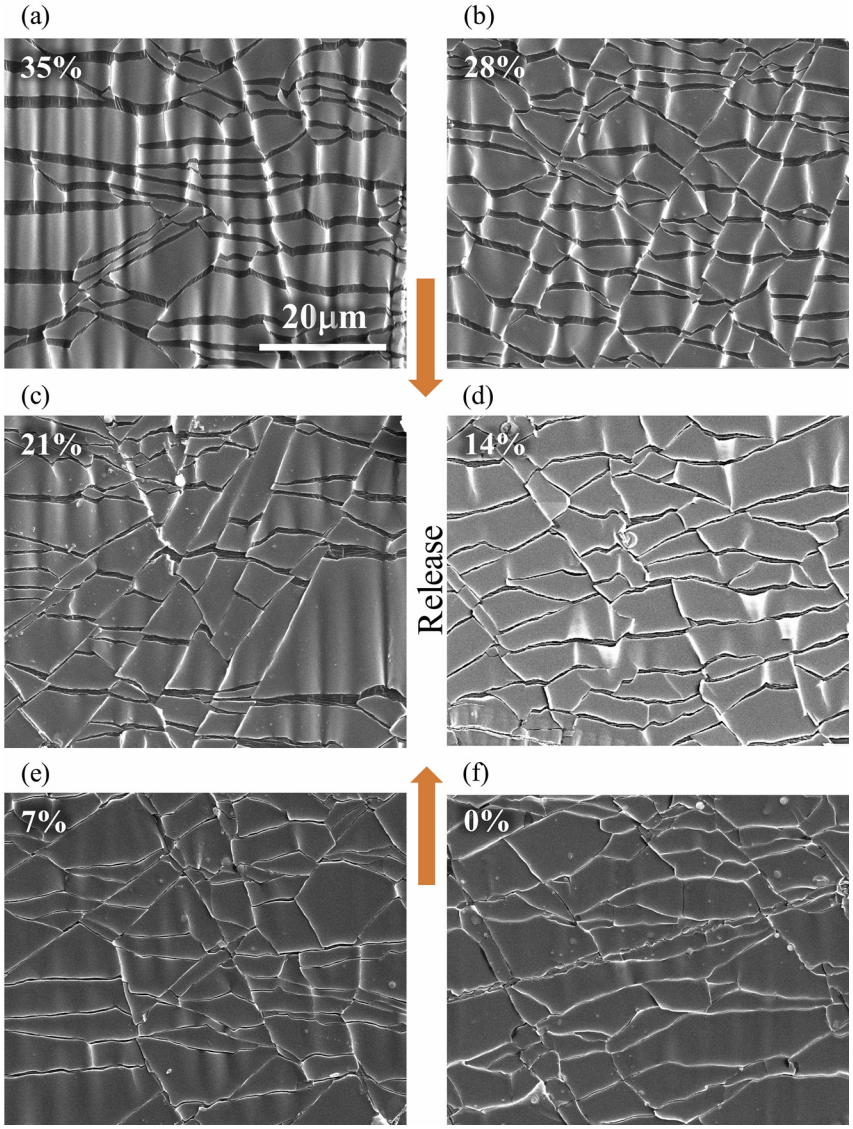

FIG. 2. SEM images of 10 nm Cr film unloaded from 35% strain to 0% strain at intervals of 7% strain ((a)–(f)). The gaps between the Cr islands are seen to reduce successively with the decreasing applied (global) strain.

Fig. 5, the cumulative width of the bands of high strain observed on the In film surface correlates very well with the widening of the gaps between the Cr islands. The absolute numbers in Fig. 5 are quantitatively different, which is attributed to the fact that the In film is much thicker than the Cr film (2.5 μm for In vs 3–5 nm for Cr) and hence the strain at the bottom of the In film (which is expected to match with the deformation of the Cr islands) is quantitatively different compared to that observed from the top.

C. Cyclic tests of In-Cr-PDMS system

The correlation between widening of gaps between the Cr islands and the strain in In interconnect film proves that the interlayer morphology plays a critical role in enabling In stretchability. This result, however, does not indicate what happens to the film resistivity when stretched and the film morphology upon release from the high strain. This is important in understanding the relationship between the overall deformation and the film electrical performance. For example, under large strain, the In film is expected to deform by elastic-plastic strain, while the PDMS elastomer is expected to deform by elastic, viscoelastic, and possibly, plastic deformation. Upon release, the elastic and viscoelastic recovery of the PDMS substrate will be significantly higher than that for In. This difference in recovery results in the formation of surface wrinkles and was reported in our prior work.[36] The surface waviness upon release from high strain can be used to delay the onset of plasticity upon subsequent cycles as long as the interfaces remain intact. Note that the plastic deformation of the In film is expected to increase the dislocation density and an increase in the resistance and resistivity. If delamination were to occur in the interlayer or the In interconnect, the film would undergo spallation. In this section, we demonstrate an approach that allows such films to be used without a deterioration in their mechanical integrity (e.g., spallation) and electrical properties (e.g., resistivity change) up to about 25% linear strain. This is achieved by applying a first strain cycle of relatively high strain amplitude followed by repeated cycles of smaller strain amplitude.

The material set chosen for this experiment was 6 μm In film on the PDMS with 3–5 nm thick Cr interlayer as stated in Section II. While stretching the In interconnect, we

Reuse of AIP Publishing content is subject to the terms at: https://publishing.aip.org/authors/rights-and-permissions. Download to IP: 69.166.45.107 On: Fri, 16 Sep 2016 15:59:33

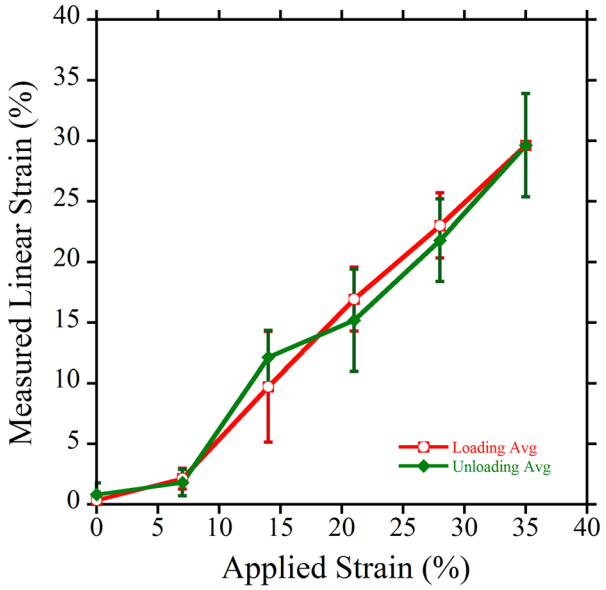

FIG. 3. Strain as measured from the width of the cracks between the Cr islands plotted against the global strain applied by the tensile stage on PDMS during the loading and unloading of Cr-PDMS system. It is concluded that the global (applied) strain is accommodated on the surface by the movement of the Cr islands.

assume that the film volume is constant as the interconnect stretching is expected to happen with plastic deformation. The resistivity, ρ, increases due to both plasticity and defects in the film, and is given by

$$\frac{\rho}{\rho_o} = \frac{R}{R_o}\left(\frac{L_o}{L}\right)^2, \tag{1}$$

where ρ_o, L_o, and R_o are the initial values of resistivity, conductor length, and resistance, and ρ, L and R are the instantaneous values of the same quantities, respectively. Here, ρ represents the effective resistivity, and any deviation of ρ/ρ_o from unity represents the combined effects of plasticity and defect formation. While doing measurements, the strain values corresponded to the linear strain in the In film and were verified by the location of the fiducial marks on the In film surface during stretching. The resistance of the film was measured *in situ* during testing by the 4-wire method. The native resistivity of the film was in the order of 10^{-8} Ω-m, close to the bulk values reported in the literature.[47]

Figures 6(a), 6(c), 6(e), 6(g) and Figs. 6(b), 6(d), 6(f), 6(h) show the R/R_o and ρ/ρ_o, respectively, for an applied strain of 65% during the first cycle, and 20%, 25%, 32%, and 38% in subsequent 10 cycles. For all the samples represented in Fig. 6, stretching the material system during the first cycle increased ρ by 1.5–1.7 times before reaching a plateau beyond about 30% strain. This behavior in the first cycle was consistent with that reported in our earlier work[36] and is believed to be due to the onset of plasticity in the initial deformation, followed by the plateau due to recovery mechanisms operating within the In film during continued deformation. The recovery can be due to dislocation rearrangement and annihilation at the surface, or due to dynamic recrystallization of the film, and is attributable to the high homologous temperature of In under ambient conditions ($T/T_m \sim 0.7$). The resistance and resistivity changes from the subsequent cycles at 20% and 25% applied strain are shown Figs. 6(a) and 6(c) and Figs. 6(b) and 6(d), respectively. It is clear that the resistivity did not increase or "ratchet" up even after 10 subsequent cycles with no indication of further rise. The resistance and resistivity changes for the second through 10th cycles with 32% and 38% strain are shown Figs. 6(e) and 6(f) and Figs. 6(g) and 6(h), respectively. The results show that the ρ/ρ_o increased after each cycle and continued to grow with subsequent cycles. The In surface did not show any signs of delamination/spallation in any of the experiments performed. In order to find the rate at which the resistivity changes for the different cyclic strains (for greater than 2 cycles), we plotted the ρ/ρ_o as a function of the number of cycles at the beginning of each cycle as shown in Fig. 7. It is clear that the resistivity shows no sign of progressive increase with the number of cycles for 20% and 25% strain, while it increases progressively for 32% and 38% strain without leveling off, confirming the observations in Figs. 6(b), 6(d), 6(f), and 6(h).

IV. DISCUSSION

The results in Figs. 1–3 establish that the deformation of PDMS-Cr interlayer interface is inhomogeneous and dominated by the Cr morphology. This is not surprising since Cr has a very high elastic modulus (181 GPa[48]) compared to that for the PDMS elastomer (0.0026 GPa[49]), even though its thickness is very small compared to the PDMS substrate. A simple calculation shows that the ratio of the force supported by Cr, if Cr were un-cracked, is comparable (~1.8 times) to that of the PDMS. This suggests that the Cr islands undergo a very low strain and the elastomer strain can be accommodated by simply moving the islands away from each other as observed from Fig. 1. Interestingly, the strain accommodation at the PDMS-Cr interface is a fully reversible process. Note that we observed little to no additional cracking in the Cr films during cycling up to a strain of 35%. Further, the Cr did not delaminate from the PDMS, indicating a strong adhesion of the film to the elastomer. Although the presence of In interconnects will affect the strain field seen in Fig. 1, the above results are a clear indication of the central role played by the brittle interlayer morphology in distributing the strain field along the length of the indium-coated elastomer as it is stretched, without allowing localization, and hence premature rupture, to occur.

In presence of the interconnect film, the cracks separating the brittle Cr islands are expected to form the buried channel cracks underneath the thick film. During substrate loading, the channel cracks can either propagate into interconnect film, causing it to rupture; or alternatively, allow interconnect film to expand freely between the expanding crack faces, depending upon the ductility of interconnect film. For example, an interconnect film with low ductility will rupture as the stress concentration caused by Cr cracks from Cr interlayer will cause them to propagate into the interconnect film. Indeed, the effect of cracking in the Cr

Reuse of AIP Publishing content is subject to the terms at: https://publishing.aip.org/authors/rights-and-permissions. Download to IP: 69.166.45.107 On: Fri, 16 Sep 2016 15:59:33

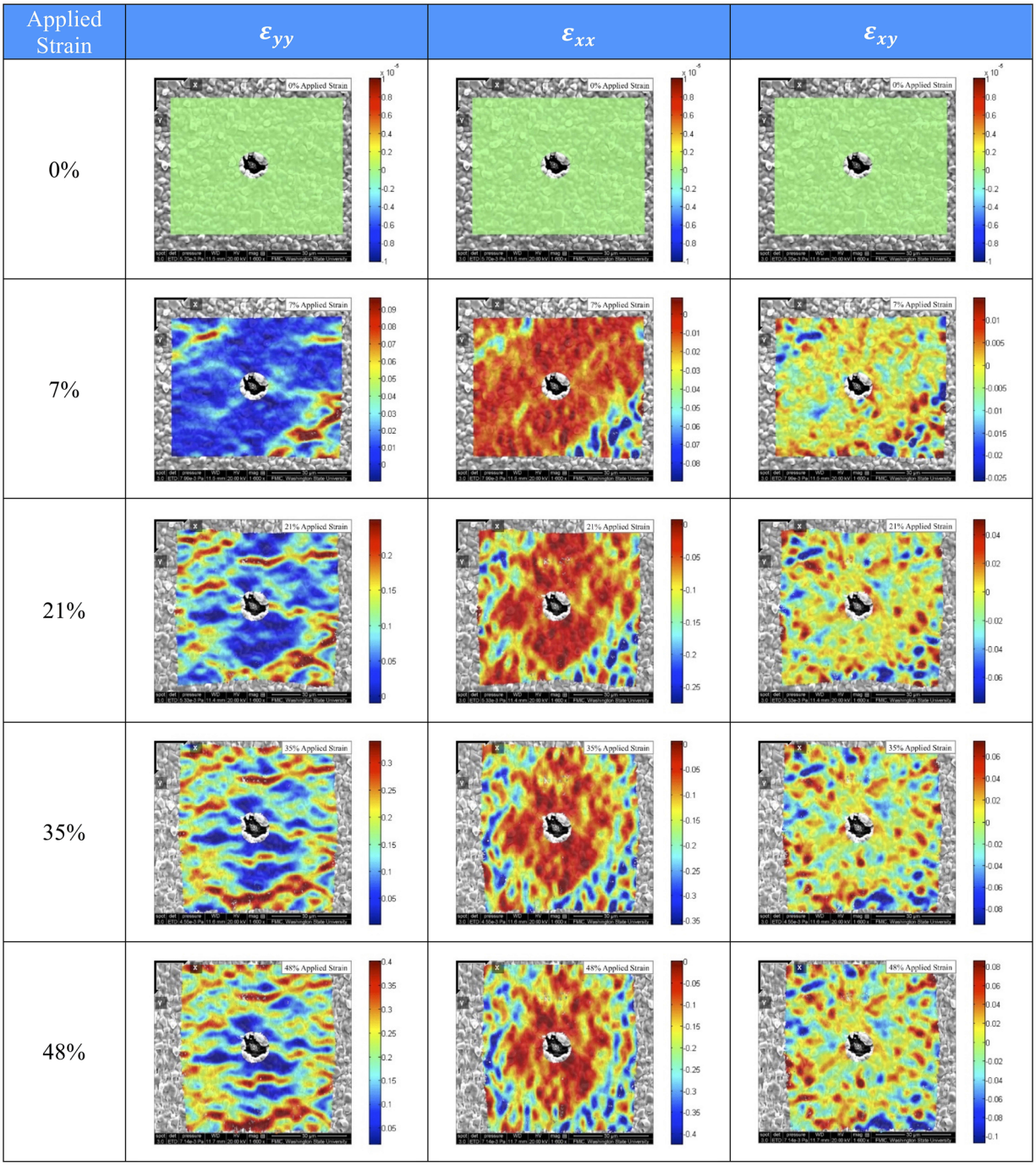

FIG. 4. The ε_{yy}, ε_{xx}, and ε_{xy} distribution on the In surface given by the DIC analysis of the SEM images at 0%, 7%, 21%, 35%, and 48% applied strain. See also the DIC images in an online video format. (Multimedia view) [URL: http://dx.doi.org/10.1063/1.4962453.1] [URL: http://dx.doi.org/10.1063/1.4962453.2] [URL: http://dx.doi.org/10.1063/1.4962453.3]

interlayer was studied for Cu interconnects and it was shown to lead to cracking and failure of the Cu interconnect film under certain loading conditions.[38] On the other hand, for highly ductile films, the widening of channel cracks from Cr interlayer results in plastic accommodation of the strain within the film, and thereby offers an opportunity for the film to expand freely between the crack faces.

The DIC results presented in Fig. 4 demonstrate that the In film deforms discontinuously with bands of high strain perpendicular to the loading direction. This periodic localization of strain in In at numerous locations (rather than at one location followed by necking and fracture) is likely responsible for the high stretchability obtained in the current system (this work and Ref. 36) by delaying the necking instability that precedes film rupture. Further, a comparison of these bands with the separation of Cr islands (Fig. 5) indicates that the deformation of the In film is driven by the discontinuous/cracked Cr interlayer. It is thus plausible that as the Cr-cracks expand under the In layer, the low yield strength (1−2 MPa), near-zero strain-hardening rate, as well as the operation of

Reuse of AIP Publishing content is subject to the terms at: https://publishing.aip.org/authors/rights-and-permissions. Download to IP: 69.166.45.107 On: Fri, 16 Sep 2016 15:59:33

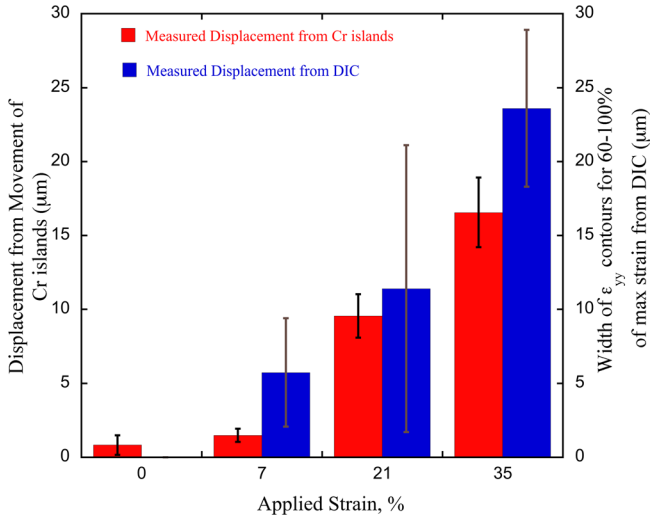

FIG. 5. Comparison between the width of cracks between the Cr islands in the Cr/PDMS system and the total width of the ε_{yy} bands of high strain on In surface (defined as regions with >60% of maximum strain for a given image) in the In/Cr/PDMS system for an applied strain of up to 35%. The cumulative width of the bands of high strain observed on the In film surface correlates very well with the widening of the gaps between the Cr islands.

creep mechanisms in In because of the high homologous temperature (~0.7 at room temperature) causes the In film to expand between the Cr islands rather than cause film rupture. In the past, de-localization of global strain in interconnect films was thought to occur only when a film was strongly bonded to the entire substrate.[28] The current work, however, establishes that global strain de-localization can be effected by numerous local localizations due to strong intermittent bonding between the film and substrate. This can delay the plastic instability (i.e. necking) and effectively impart substantial ductility to the metal film.

We next discuss the implications of the resistance and resistivity results shown in Figs. 6(a)–6(h). During loading of the interconnect in the first cycle, all the plots show a rise in resistivity which is a result of the damage accumulation in the form of (i) dislocations required to accommodate plastic strain resulting in higher resistance to the current flow, and (ii) possible micro-cracking that results in a reduction of the effective cross section area for the current flow. The rise in resistivity is seen to plateau at a strain >30%, consistent with the observations in our prior work.[36] Reaching a plateau suggests that recovery/recrystallization mechanisms in low melting temperature materials such as In can limit the rise in the dislocation density. The result also indicates that micro-cracking (which would be expected to increase with loading) is likely not the primary source in the rise in the film resistivity. Thus, the strategies to arrest the rise in resistivity are to either delay the onset of plasticity or to induce recovery/recrystallization mechanisms in the film at a lower strain. In case of the strain of 20% and 25% from the second cycle, the wrinkles formed at the end of the first cycle are expected to straighten without putting the film in plastic deformation and hence an increased density of dislocations. This is indeed observed with no rise in resistivity even after 10 strain cycles. In case of a strain of 32% and 38%, it is likely that the film enters the plastic regime at some point after the wrinkles are straightened and the resistivity rises due to an increase in the dislocation density. Again, we see a rise in resistivity with repeated cycling. Thus, although the overall strain for the cycle 2–10 is 38% for Figs. 6(g) and 6(h), the linear strain is likely to be less than 38%. Figures 6(a)–6(h) also clarify several features of the deformation of the interconnect system. For example, during unloading, the resistivity appears to increase at lower strain (e.g., Fig. 6(d)). This is likely to be an artifact as the out-of-plane wrinkles at lower strain can increase the conductor-length, which is not taken into account in resistivity calculations. The graph can thus be used to identify when the out of plane wrinkles start to form in the In film. Note that the advantage of the engineered out-of-plane wrinkles by stretching the In interconnect to high strain in the first cycle is that this method will allow patterning of the films to high density prior to the wrinkle formation. Visual observations and results in Figs. 6 and 7 also indicate that the In films do not peel off from the substrate during repeated cycling. The results in Figs. 6 and 7 also demonstrate that the onset of plasticity can be delayed in the interconnect films using the strain mismatch in the first loading cycle.

The resistivity vs. deformation graphs observed in the experimental results discussed above establish that the mechanism of stretching of a highly ductile film on an elastomer substrate with a brittle adhesion interlayer consists of the following steps:

(i) When PDMS is stretched, the separation of islands of the already cracked Cr interlayer islands occurs underneath the thicker In.
(ii) The In remains bonded to the Cr islands and expands in localized bands of deformation above the separating Cr blocks/islands
(iii) Since the strain in In film is distributed throughout the contact plane, its failure is delayed since no single region can easily form a neck, a necessary condition for film rupture.
(iv) Although the deformation of Cr-PDMS is elastic, In undergoes a permanent (plastic) deformation at high strain, resulting in a strain mismatch during the unloading cycle. This results in the wavy surface morphology of such films upon unloading. This phenomenon can be used to engineer interconnect systems that can be stretched at least up to 25% linear strain without a deterioration of their electrical performance.

The current work explains the physical processes that help accommodate large linear strain in metallic interconnects on elastomer substrates. We note, however, that nanoscale processes within metallic films that lead to the large local strains above the cracks in the Cr-interlayer are not fully understood and need further investigation, possibly via *in situ* straining experiments in the transmission electron microscope. Additionally, the recovery/recrystallization processes that help prevent a rise in the film resistivity at high strains, as shown in Fig. 6, need further research. A full understanding of the mechanisms of stretching can then be

Reuse of AIP Publishing content is subject to the terms at: https://publishing.aip.org/authors/rights-and-permissions. Download to IP: 69.166.45.107 On: Fri, 16 Sep 2016 15:59:33

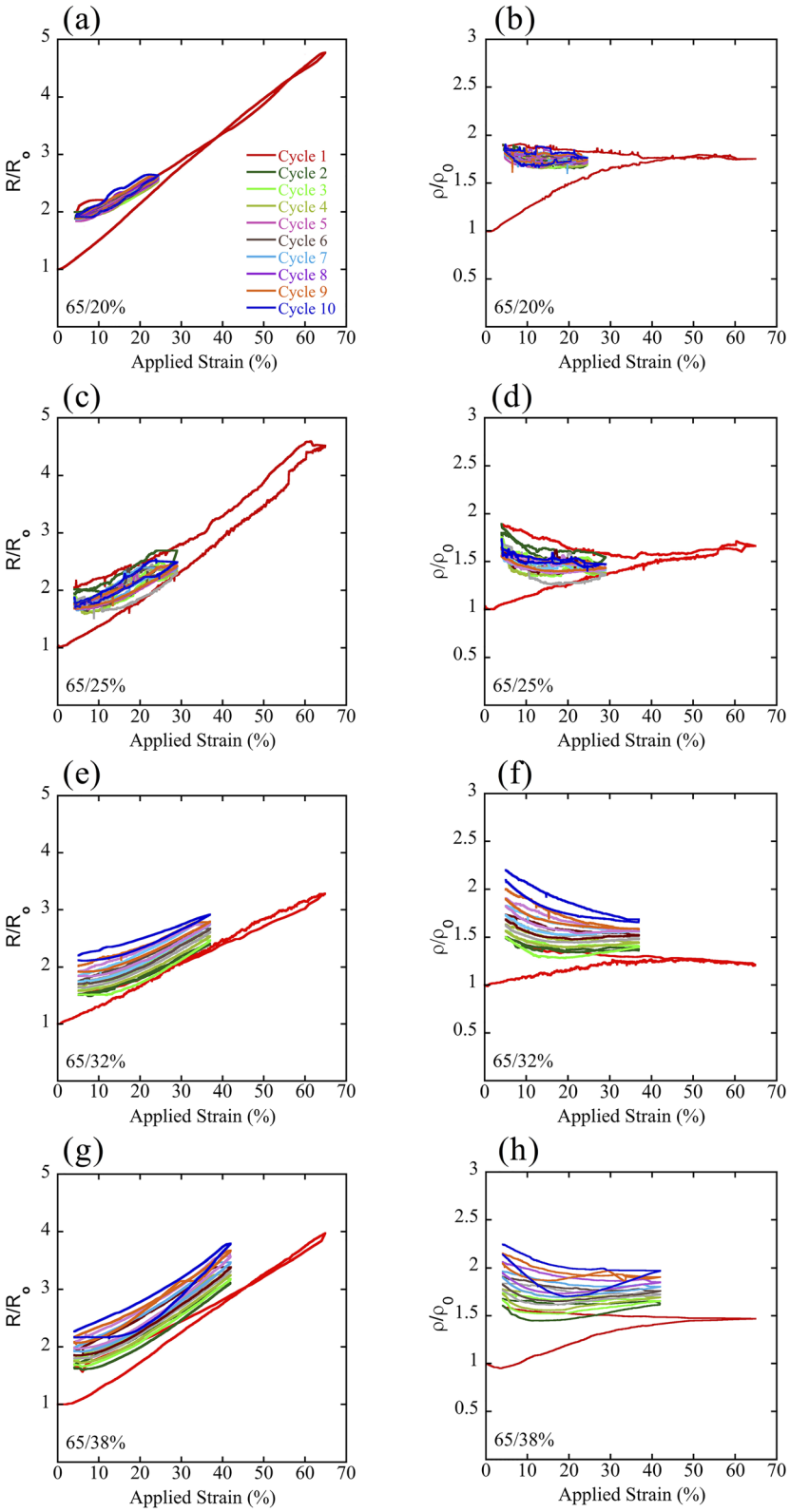

FIG. 6. Change in resistance and resistivity for samples with 1st cyclic loading at 65% strain followed by repeated cyclic strain of ((a) and (b)) 20%, ((c) and (d)) 25%, ((e) and (f)) 30%, ((g) and (h)) 38% for the next 9 cycles. All the samples have been tested at a strain rate of $\sim 1.3 \times 10^{-3}$/s.

used to engineer low-cost material systems to create interconnects that meet the demanding industry requirements.

V. SUMMARY AND CONCLUSIONS

In this paper, we present experimental results that clarify the mechanisms of stretching for ductile interconnect films on elastomer substrates with a discontinuous adhesion interlayer. We show that:

(1) The thin adhesion interlayer has a cracked morphology that causes a delay in the necking and fracture of the interconnect film by causing the film strain to localize at numerous locations along the entire surface as the elastomer is stretched to a high strain.

Reuse of AIP Publishing content is subject to the terms at: https://publishing.aip.org/authors/rights-and-permissions. Download to IP: 69.166.45.107 On: Fri, 16 Sep 2016 15:59:33

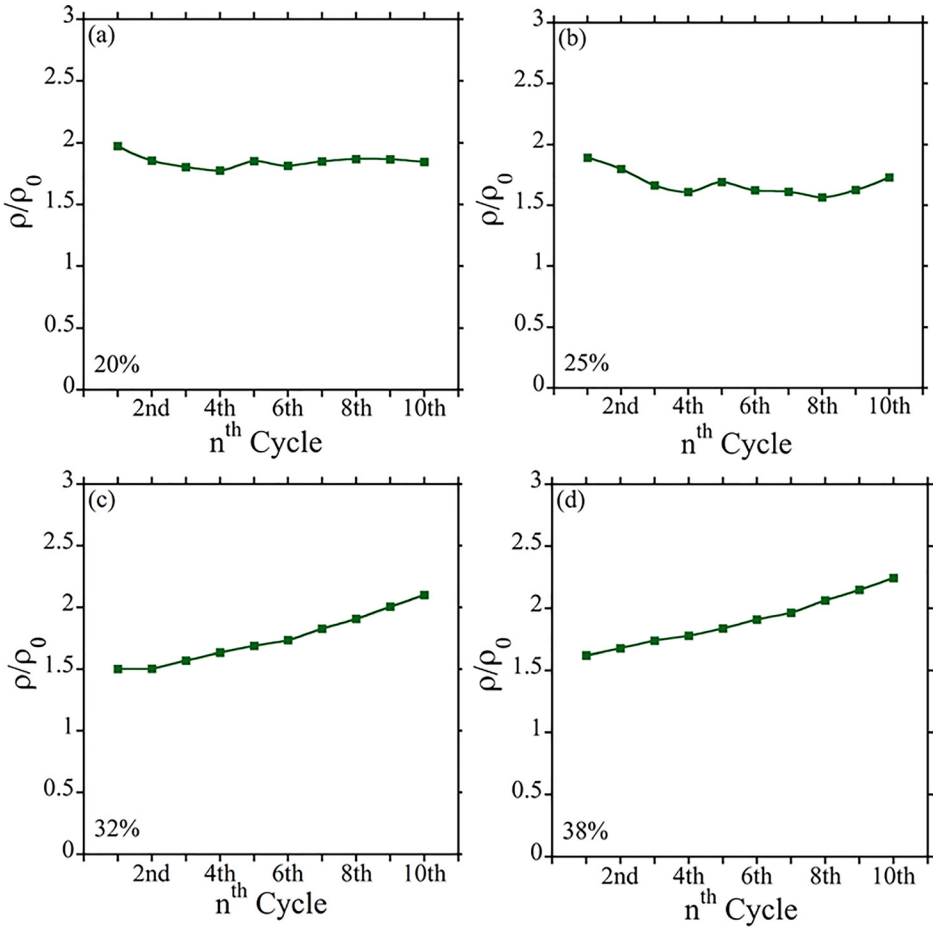

FIG. 7. Change in resistivity with a number of cycles for samples with 65% first cyclic strain each followed by (a) 20% (b) 25% (c) 30% and (d) 38% strain range. For samples (a) and (b), there is no significant increase in resistivity whereas for samples (c) and (d) the rise is remarkable with increasing number of cycles.

(2) The interconnect system develops out of plane wrinkles when released from high strain in the first cycle due to lack of full strain-recovery of the plastically deformed In, coupled with full elastic strain-recovery of the elastomer substrate.
(3) The electrical degradation of interconnect films as a function of applied strain can be arrested by either delaying the onset of plasticity through geometrical features such as wrinkles, or, triggering recovery and/or recrystallization mechanisms in the interconnect film at a lower strain.
(4) By inducing large strains in the In film at numerous locales corresponding to the cracks in the Cr-interlayer and by inducing surface wrinkles during release from the first straining cycle. In interconnect films can be engineered to stretch up to 25% linear strain without a deterioration of their electrical properties.

ACKNOWLEDGMENTS

The work was supported by R.P.'s start-up fund at WSU. We thankfully acknowledge the support from Joshah Jennings, Robert Lentz, the mechanical workshop, and Franceschi Microscopy and Imaging Center (FMIC) at WSU.

[1]R. D. Ponce Wong, J. D. Posner, and V. J. Santos, Sens. Actuators, A **179**, 62 (2012).
[2]H. C. Ko, M. P. Stoykovich, J. Z. Song, V. Malyarchuk, W. M. Choi, C. J. Yu, J. B. Geddes, J. L. Xiao, S. D. Wang, Y. G. Huang, and J. A. Rogers, Nature **454**, 748 (2008).
[3]D. H. Kim, N. S. Lu, R. Ma, Y. S. Kim, R. H. Kim, S. D. Wang, J. Wu, S. M. Won, H. Tao, A. Islam, K. J. Yu, T. I. Kim, R. Chowdhury, M. Ying, L. Z. Xu, M. Li, H. J. Chung, H. Keum, M. McCormick, P. Liu, Y. W. Zhang, F. G. Omenetto, Y. G. Huang, T. Coleman, and J. A. Rogers, Science **333**, 838 (2011).
[4]S. Scataglini, G. Andreoni, and J. Gallant, in *A Review of Smart Clothing in Military* (ACM, 2015), p. 53.
[5]N. M. Farandos, A. K. Yetisen, M. J. Monteiro, C. R. Lowe, and S. H. Yun, Adv. Healthcare Mater. **4**, 792–810 (2015).
[6]B. C. K. Tee, A. Chortos, R. R. Dunn, G. Schwartz, E. Eason, and Z. Bao, Adv. Funct. Mater. **24**, 5427 (2014).
[7]Y. Chen, J. Au, P. Kazlas, A. Ritenour, H. Gates, and M. McCreary, Nature **423**, 136 (2003).
[8]G. H. Gelinck, H. E. A. Huitema, E. Van Veenendaal, E. Cantatore, L. Schrijnemakers, J. Van der Putten, T. C. T. Geuns, M. Beenhakkers, J. B. Giesbers, B. H. Huisman, E. J. Meijer, E. M. Benito, F. J. Touwslager, A. W. Marsman, B. J. E. Van Rens, and D. M. De Leeuw, Nat. Mater. **3**, 106 (2004).
[9]B. Yoon, D. Y. Ham, O. Yarimaga, H. An, C. W. Lee, and J. M. Kim, Adv. Mater. **23**, 5492 (2011).
[10]E. Kim, H. Tu, C. Lv, H. Jiang, H. Yu, and Y. Xu, Appl. Phys. Lett. **102**, 033506 (2013).
[11]J. A. Rogers, T. Someya, and Y. Huang, Science **327**, 1603 (2010).
[12]T. Someya, *Stretchable Electronics* (John Wiley and Sons, 2012).
[13]S. P. Lacour, J. Jones, S. Wagner, T. Li, and Z. Suo, Proc. IEEE **93**, 1459 (2005).
[14]H. Yung-Yu, K. Lucas, D. Davis, B. Elolampi, R. Ghaffari, C. Rafferty, and K. Dowling, IEEE Trans. Electron Devices **60**, 2338 (2013).
[15]Y.-Y. Hsu, M. Gonzalez, F. Bossuyt, F. Axisa, J. Vanfleteren, and I. De Wolf, J. Micromech. Microeng. **20**, 075036 (2010).
[16]R. Taylor, C. Boyce, M. Boyce, and B. Pruitt, J. Micromech. Microeng. **23**, 105004 (2013).

Reuse of AIP Publishing content is subject to the terms at: https://publishing.aip.org/authors/rights-and-permissions. Download to IP: 69.166.45.107 On: Fri, 16 Sep 2016 15:59:33

[17]Y. Zhang, H. Fu, Y. Su, S. Xu, H. Cheng, J. A. Fan, K.-C. Hwang, J. A. Rogers, and Y. Huang, Acta Mater. **61**, 7816 (2013).
[18]Y. Zhang, S. Wang, X. Li, J. A. Fan, S. Xu, Y. M. Song, K. J. Choi, W. H. Yeo, W. Lee, and S. N. Nazaar, Adv. Funct. Mater. **24**, 2028 (2014).
[19]O. V. D. Sluis, Y. Y. Hsu, P. H. M. Timmermans, M. Gonzalez, and J. P. M. Hoefnagels, J. Phys. D: Appl. Phys. **44**, 034008 (2011).
[20]M. Jablonski, F. Bossuyt, J. Vanfleteren, T. Vervust, and H. de Vries, Microelectron. Reliab. **53**, 956 (2013).
[21]M. Gonzalez, B. Vandevelde, W. Christiaens, Y.-Y. Hsu, F. Iker, F. Bossuyt, J. Vanfleteren, O. Van der Sluis, and P. Timmermans, Microelectron. Reliab. **51**, 1069 (2011).
[22]S. Béfahy, S. Yunus, T. Pardoen, P. Bertrand, and M. Troosters, Appl. Phys. Lett. **91**, 141911 (2007).
[23]D.-Y. Khang, H. Jiang, Y. Huang, and J. A. Rogers, Science **311**, 208 (2006).
[24]C. Lv, H. Yu, and H. Jiang, Extreme Mech. Lett. **1**, 29–34 (2014).
[25]H. Yung-Yu, P. Cole, L. Daniel, W. Xianyan, R. Milan, Z. Baosheng, and G. Roozbeh, J. Micromech. Microeng. **24**, 095014 (2014).
[26]S. Wagner and S. Bauer, MRS Bull. **37**, 207 (2012).
[27]C. Mack, *Fundamental Principles of Optical Lithography: The Science of Microfabrication* (John Wiley and Sons, 2008).
[28]T. Li, Z. Huang, Z. Xi, S. P. Lacour, S. Wagner, and Z. Suo, Mech. Mater. **37**, 261 (2005).
[29]N. Lu, X. Wang, Z. Suo, and J. Vlassak, Appl. Phys. Lett. **91**, 221909 (2007).
[30]T. Li and Z. Suo, Int. J. Solids Struct. **43**, 2351 (2006).
[31]C. Tsay, S. P. Lacour, S. Wagner, T. Li, and Z. Suo, in *How Stretchable Can We Make Thin Metal Films?* (Cambridge University Press, 2005), p. O5.5.
[32]Y. Xiang, T. Li, Z. Suo, and J. J. Vlassak, Appl. Phys. Lett. **87**, 161910 (2005).
[33]J. Jones, S. P. Lacour, S. Wagner, and Z. Suo, J. Vacuum Sci. Technol. A **22**, 1723 (2004).
[34]O. Akogwu, D. Kwabi, S. Midturi, M. Eleruja, B. Babatope, and W. O. Soboyejo, Mater. Sci. Eng. B **170**, 32 (2010).
[35]H. Vandeparre, Q. Liu, I. R. Minev, Z. Suo, and S. P. Lacour, Adv. Mater. **25**, 3117 (2013).
[36]Y. Arafat, I. Dutta, and R. Panat, Appl. Phys. Lett. **107**, 081906 (2015).
[37]T. Ye, Z. Suo, and A. Evans, Int. J. Solids Struct. **29**, 2639 (1992).
[38]V. M. Marx, F. Toth, A. Wiesinger, J. Berger, C. Kirchlechner, M. J. Cordill, F. D. Fischer, F. G. Rammerstorfer, and G. Dehm, Acta Mater. **89**, 278 (2015).
[39]R. Mahajan, P. Brofman, R. Alapati, C. Hilbert, L. Nguyen, K. Maekawa, M. Varughese, D. O'Connor, S. Ramaswami, and J. Candelaria, *Packaging Needs Document* (Semiconductor Research Corporation (SRC), 2015), available at https://www.src.org/program/grc/pkg/research-needs/2015/packaging.pdf.
[40]S. L. Peterson, A. McDonald, P. L. Gourley, and D. Y. Sasaki, J. Biomed. Mater. Res. Part A **72A**, 10 (2005).
[41]D. Bodas and C. Khan-Malek, Sens. Actuators, B **123**, 368 (2007).
[42]J. Blaber, B. Adair, and A. Antoniou, Exp. Mech. **55**, 1105 (2015).
[43]R. Harilal and M. Ramji, "Adaptation of open source 2D DIC software Ncorr for solid mechanics applications," in Proceedings of the 9th International Symposium on Advanced Science and Technology in Experimental Mechanics, 1–6 November 2014, New Delhi, India.
[44]J. Blaber and A. Antoniou, "Ncorr instruction manual," see http://www.ncorr.com/download/ncorrmanual_v1_2_1.pdf (2015).
[45]C. A. Schneider, W. S. Rasband, and K. W. Eliceiri, Nat. Methods **9**, 671 (2012).
[46]M. D. Abramoff, P. J. Magalhães, and S. J. Ram, Biophotonics Int. **11**, 36 (2004).
[47]R. Fogelholm, Ö. Rapp, and G. Grimvall, Phys. Rev. B **23**, 3845 (1981).
[48]K. E. Petersen and C. R. Guarnieri, J. Appl. Phys. **50**, 6761 (1979).
[49]Z. Wang, A. A. Volinsky, and N. D. Gallant, J. Appl. Polym. Sci. **131**, 41050 (2014).

Reuse of AIP Publishing content is subject to the terms at: https://publishing.aip.org/authors/rights-and-permissions. Download to IP: 69.166.45.107 On: Fri, 16 Sep 2016 15:59:33